Reconsidering the potential of micropyrolyzer to investigate biomass fast pyrolysis without heat transfer limitations

Manel Nasfi, Marion Carrier, Sylvain Salvador

Reconsidering the potential of micropyrolyzer to investigate biomass fast pyrolysis without heat transfer limitations

Manel Nasfi, Marion Carrier *, Sylvain Salvador

RAPSODEE, CNRS UMR 5203, Université de Toulouse, IMT Mines Albi, Campus Jarlard, 81013 Albi CT, Cedex 09, France

A B S T R A C T

Commercial analytical pyrolysis systems have become increasingly used in biomass fast pyrolysis research. Establishing experimental conditions free from heat transfer limitations using these micro-rectors has not been verified. Since accurate measurement of biomass sample temperature with these devices is not possible, the isothermal character of experiments has never been verified. In this work, numerical simulations were conducted to assess the time-temperature history of both cup and different sample arrangements and to determine the overall heat transfer coefficients at the surface of the biomass samples to confirm the pyrolysis regime based on the dimensionless analysis in the micropyrolyzer. Using both a small mass of biomass sample ($\leq$ 50 µg) carefully arranged at the bottom of the cup and a temperature below 723 K allows the complete elimination of heat transfer limitations within the micropyrolyzer. The heating time of the biomass sample was significant (4–5 s to reach 773 K), proving that the experiment is not isothermal. Thus, evaluating the kinetics of biomass fast pyrolysis requires establishing the time-temperature history of the sample, as an essential prerequesite. Both heating profiles of biomass samples arranged in thin-film and torus were found to follow that of the cup; the time-temperature history of the sample can be determined by measuring the temperature of the cup.

1. Introduction

Pyrolysis is a flexible technology that allows the production of bio-oil, biochar, and gas by selecting the appropriate pyrolysis and quenching operational parameters [1]. To mainly produce liquid, fast heating (500 K/s) of small biomass particles ($<$ 3 mm) and short volatiles residence time ($<$ 2 s) without adding oxygen are required [2]: 'fast' pyrolysis is the conventional name of this process. The rapid quenching of volatiles leads to a dark brown liquid called pyrolytic oil or bio-oil. Pyrolytic oil has the advantage of being easily stored and transported, being a source of commodity and high-value chemicals [3,4], and being used as transportation liquid fuels [5]. The potential of bio-oil is increasingly recognized, with a growing number of researches focusing on modeling approaches to the fast pyrolysis process and bio-oil upgrading technologies [6–8]. Studying kinetics of biomass pyrolysis is essential for designing reactors and optimizing the global process [9]. These works can help to improve the selectivity of desired products. Conducting the chemical kinetics of biomass pyrolysis requires isolating the primary reactions from both undesirable reactions and transport phenomena [10]. This task is challenging because of the complex nature of biomass fast pyrolysis: the solid biomass softens and polymeric chains are depolymerized and fragmented to form a reactive intermediate (composed of oligomers) that bubbles when volatile products are formed via secondary reactions [11–13]. Indeed, solid and liquid phase chemistries can be convoluted with intertwined transport phenomena that lead to heat and mass transfer limitations. Therefore, researchers must master the experimental equipment, control the pyrolysis conditions and provide suitable methods to evaluate the pyrolysis chemistry. The choice of the experimental technique is one of the most critical decisions that must be made to ensure efficient heat transfer. The most common equipment used for studying pyrolysis kinetics is the thermogravimetric analyzer (TGA). However, the typical heating rates of TGA (0.01–1.66 K/s) are not suitable to study fast pyrolysis [14,15]. Other reactors, such as the PHASR reactor [16] and wire mesh reactor [17,18], can reach controlled and high heating rates, up to 12,000 and 7000 K/s, respectively. Although the PHASR represents a real progress to measure high temperature millisecond-scale solid state reactions [19], its access remains still limited. Therefore, most of the published studies of biomass fast pyrolysis involve commercial micro-reactors such as the downflow micro-furnace pyrolyzer [20–25], the curie-point

* Corresponding author.
E-mail address: marion.carrier@mines-albi.fr (M. Carrier).

Table 1
Kinetic parameters for biomass fast pyrolysis (adapted from [41,42]).

Reference	Feedstock	Initial mass (mg)	Experimental system	Temperature (K)	Activation energy (kJ.mol^{-1})	Pre-exponenetial factor (s^{-1})
Brink and Massoud [43]	White fir (<0.175 mm)	–	Drop-tube furnace	920–1144	105	2.64×10^{5}
Thurner and Mann [44]	Oak sawdust (1000 μm)	–	Horizontal tube furnace	573–673	106.5	1.481×10^{6}
Pyle and Zaror [45]	Pine (0.6–2.2 cm)	–	TGA	653–773	66	2.00×10^{3}
Font et al. [46]	Almond shells (300–500 μm)	–	Pyroprobe	733–878	108	1.89×10^{6}
Wagenaar et al. [47]	Pine (100–125 μm)	1 – 7	TGA Drop-tube furnace	573–723 723–873	150	1.40×10^{10}
Di Blasi and Branca [48]	Beech (<80 μm)	9	TGA		141	4.40×10^{9}
	Beech (100–500 μm)	35×10^{3} - 40×10^{3}	Horizontal tube furnace	573–708	95.4	2.40×10^{5}
Biagini et al. [30]	Olive residue (pulverized)	5–20	Pyroprobe	< 1673	114	3.27×10^{6}
Zhu et al. [41]	α-cyclodextrin (thin-film <10 μg)	0.05	PHASR reactor	658–740 740–778	97.1 224.7	2.00×10^{7} 2.40×10^{16}

pyrolyzer [26–28], and the resistive filament pyrolyzer [29,30]. The primary technical challenge in using commercial reactors is to make accurate measurements of the actual temperature of biomass sample. Knowing the time-temperature history within the sample is critical to assessing the chemical modeling of biomass fast pyrolysis[31]. The determination of the actual heating rates of the biomass sample remains ambiguous. In most cases, researchers indicate the heating rates of the heating elements rather than the sample [32–34]. Some authors assume that pyrolysis occurs under a linear heating rate [30,35]. In this context, Maduskar et al. [16] presented five requirements for measuring intrinsic isothermal biomass fast pyrolysis kinetics: 1) use of small biomass characteristic lengths (< 10 μm); 2) direct measurement of the biomass sample; 3) application of fast heating rate of biomass sample to avoid biomass conversion during temperature rise; 4) record of the progression of reaction with time and minimal mixing of vapors and gases during their transfer from the pyrolysis reactor to the detector when using an online detection method (or with fast cooling of a solid sample when using the quenching reacting solid sample method); 5) and use of high carrier gas flow rates to minimize products residence time and avoid secondary reactions. The authors have concluded that the PHASR reactor satisfied these five criteria and is suitable for measuring intrinsic isothermal kinetics. According to the authors, both downflow and horizontal flow micropyrolyzers fail to fulfill the fast heating requirement. In our opinion, the statute of this statement should be reassessed as detailed kinetics studies can be carried out in isothermal and dynamic experiments[36]. Incorporating the time-temperature history of the sample into the kinetic analysis takes into account the biomass conversion during the temperature rise. Seeking to know the time-temperature history of the biomass sample in a micropyrolyzer is one of the motivations of this paper.

Regardless of their origin, lignocellulosic biomass typically presents a low thermal conductivity, 0.23 W.m^{-1}. K^{-1} [37]; it is not adapted for efficient conduction of heat. This is why sample preparation techniques such as powdered and thin-film samples have been used to minimize heat transfer limitations by decreasing the characteristic lengths of samples. In analytical microreactors, samples are generally reduced to powders; as a result, the effect of initial mass on product distribution is checked. Patwardhan et al. [20] studied cellulose fast pyrolysis in an analytical horizontal flow reactor, the pyroprobe. They did not find any difference in the distributions of products when they varied the initial mass of cellulose between 200 and 800 μg. This was later confirmed by Zang et al. [38], who used a similar micropyrolyzer and recommended using fewer than 800 μg of biomass sample to minimize heat and mass transfer limitations and ensure a pure kinetic regime.

On the other hand, Dauenhauer et al. demonstrated in few studies [16,39–41] by analyzing the product distribution and the dimensionless numbers that pyrolysis of thin-film (<10 μm) is required to ensure an isothermal kinetically-controlled regime. The thin-film technique involves the preparation of a sample suspension in the water, which is subsequently removed by evaporation, leaving behind a micro-scale film corresponding to 50 μg of biomass sample. It is unknown whether this preparation step can influence chemical kinetics. In parallel to the experimental study on transport limitations, the dimensionless analysis must be carried out to ensure control of the pyrolysis regime.

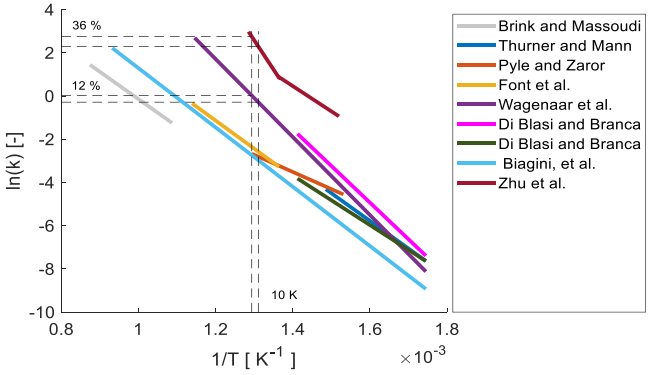

Fig. 1. Arrhenius plot for biomass pyrolysis (same data as Table 1).

Values of the reaction rate constants are required for pyrolysis numbers calculation. It becomes then critical to select the right value essential to represent the intrinsic kinetics of the pyrolysis chemical reactions. Single-step models are generally used for the pyrolysis numbers calculation, and those classic representations of biomass fast pyrolysis are summarized in Table 1 and displayed in Fig. 1.

When comparing studies, a considerable variation in activation energy (66–224.7 kJ.mol^{-1}) and pre-exponential factor (2×10^{3} to 2.4×10^{16} s^{-1}) was observed. Those disparities are usually due to the heterogeneity of the biomass, the different operating conditions, and the heating conditions established in diverse reactors [49]. Heat transfer limitations can influence chemical kinetics. When using large particles or high amounts of biomass samples, a large thermal gradient appears within the sample. On the other hand, small particle sizes or small amounts of samples lead to a homogenous overall sample temperature that flows to the reactor temperature. The higher the inhomogeneity in the biomass sample, the lower the activation energy [9].

The Arrhenius plot (Fig. 1) represents those diverse conditions for biomass pyrolysis and confirms that the kinetic parameters determined using the PHASR reactor provide the fastest conversion at a low-temperature range. The high reaction rates derived from the PHASR guarantee the kinetic control compared to the other studies. In addition, a slight temperature change of 10 K increases the kinetic constant by

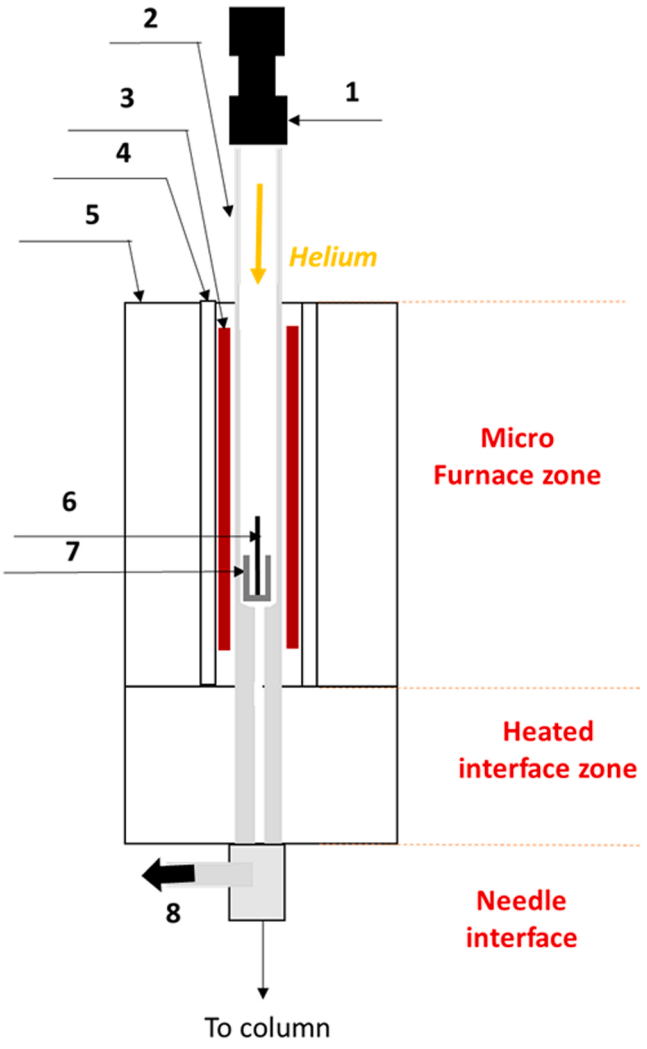

Fig. 2. Schematic description of the pyrolyzer. 1: sampler, 2: reactor (Quartz tube), 3: heating sleeve, 4: ceramic support, 5: Porex insulator, 6: stick, 7: cup, and 8: split vent.

12% for the study carried out by Pyle and Zaror [50] and up to 36% for that carried out by Zhu et al. [41]. This demonstration indicates three facts: (1) that it is difficult to judge the isothermal nature of the sample without fixing the limit of temperature difference within the sample that does not significantly impact the kinetics, (2) mass and heat transfer limitations can lead to wrong kinetics, (3) and that it is critical to use suitable and intrinsic kinetic parameters for pyrolysis to ensure the best indications for the rate-controlling process.

One of the most critical and hard to evaluate parameters that are used to calculate the values of the dimensionless numbers is the external heat transfer coefficient. There is no information about the actual heat transfer coefficient in the commercial pyrolyzers in the literature due to the challenges of measuring it. In addition, the heat transfer performances in commercial micro-reactors are not fully understood by users because of the complexity and the non-availability of their exact characteristics and configurations. Carrier et al. [51] used the value of 500 $W.m^{-2}.K^{-1}$ for heat transfer coefficient, which is usually used for spherical biomass particles in the fluidized bed reactor, to estimate the reaction-transport regime for the pyroprobe. To assess the heat transfer coefficient for particles in a micropyrolyzer, Paulsen et al. [40] proposed an averaged value of 2000 $W.m^{-2}.K^{-1}$ based on the work of Dauenhauer et al. [13] and Papadikis and Bridgwater [52], who respectively used an ablative reactor ($U=10^4$ to 10^5 $W.m^{-2}.K^{-1}$) and a fluidized bed reactor ($U=500$ $W.m^{-2}.K^{-1}$). Considering the wide variety of these values, it becomes essential to determine the value of the heat transfer coefficient at the interface of the biomass sample in the experimental device in use. Zhang et al. [38] applied empirical correlations for forced convection to calculate the convective heat transfer for the cup and the sample in a pyroprobe. Proano et al. [35] have also used similar correlations to simulate heat transfer in the micro-pyrolyzer. Empirical correlations only apply to regular geometric shapes, such as plates, cylinders, and spheres. In addition, there are still doubts about the applicability of conventional macro-scale correlations to micro-scale systems [53]. Moreover, radiative heat transfer may become significant at higher temperatures and is not included in such correlations. Instead, the heat transfer coefficients can be determined by simulations that combine the fluid flow dynamics with the heat transfer phenomenon [54,55]. However, this technique is very demanding in terms of calculation [54].

The experimental determination of the temperature of the biomass sample and the overall heat transfer coefficient at its surface is challenging, and this uncertainty can lead to incorrect kinetic constants. The incapacity of characterizing the transport phenomena within and around the biomass sample has limited the understanding of the detailed mechanism of biomass pyrolysis [56].

The main objective of this study was to establish the typical operating conditions to conduct kinetics in the absence of heat transfer limitations within the micropyrolyzer. Computational fluid dynamics (CFD), which is an effective tool to reveal the underlined mechanisms at particle and reactor scales [57], was used. A thorough heat transfer study has enabled the assessment of the time-temperature history of both cup and sample. The determination of the overall heat transfer coefficient at the surface of the biomass sample, and further critical discussions on the pyrolysis regime were proposed. The conditions in which experiments without heat transfer limitations can be performed in the micropyrolyzer were established.

2. Methodology

2.1. Apparatus

This study investigates heat transfers in the furnace-based micropyrolyzer (EGA/Py-3030D; Frontier lab). This commercial micro-rector can ensure fast biomass heating and can be easily coupled to analytical instrumentations such as gas chromatographer and mass spectrometer. Fig. 2 shows the schematic of the micropyrolyzer, which consists of a sampler that holds samples, the reactor made in Quartz, heating sleeve, ceramic support, Porex insulator, and a heated interface zone to keep the pyrolysis products in the gaseous state until they reach the GC injector.

A stainless steel stick suspends the deactivated stainless-steel cup containing a biomass sample at the top of the reactor tube. The stick and the cup containing the biomass are liberated in the preheated zone by pressing a button on the top of the sampler. The change in Quartz tube diameter (from 4.8 to 1.9 mm) supports the cup (I.D = 3.6 mm, O.D = 4 mm, and length = 5 mm) and keeps it in the center of the hot zone. The helium flows from the top of the reactor to the GC injector entraining gases released from the pyrolysis of biomass sample. After splitting, a fraction of evolved gases flows to the detector through a deactivated capillary tube (EGA tube, I.D = 0.15 mm and length = 2.5 m).

2.2. Measurement of cups temperatures

The system indicates only the temperature of the heating sleeve; the actual temperature of the cup should be measured by other means. A direct thermocouple (type K and 0.25 mm in diameter; TC S.A.), which was connected to the Agilent 34970 A acquisition unit, was used. When the pyrolyzer furnace temperature had stabilized at 773 K, the thermocouple and the cup were manually introduced inside the micro-reactor.

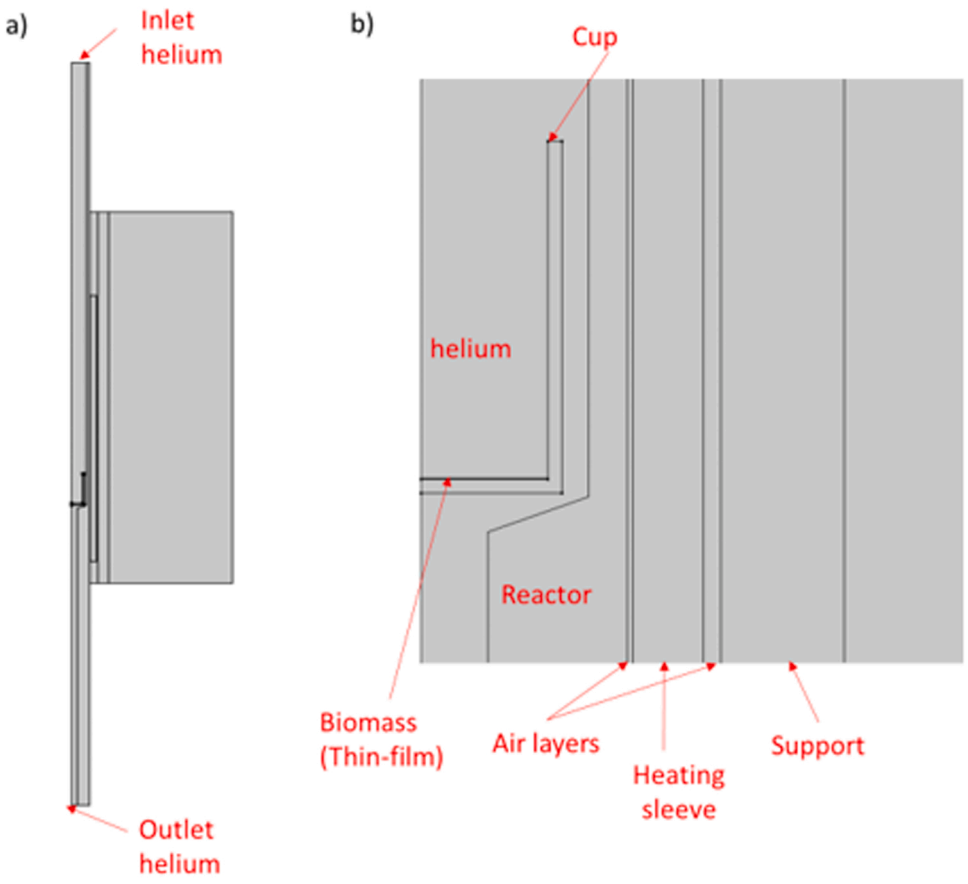

Fig. 3. a) Components of the micropyrolyzer as described in the simulation. b) Expanded view of 2D geometry, which clearly shows the cup containing the biomass sample inside the Quartz tube, as well as its placement relative to the Quartz tube.

2.3. Numerical model and simulation

COMSOL Multiphysics® v5.5 based on the finite element method has been used for this study with a consideration of the following hypotheses: (1) a 2D axisymmetric geometry is used; (2) the absence of chemical reactions; (3) the flow is assumed to be laminar; (4) air layers located between the Quartz tube and the heating sleeve and between the insulator and the heating sleeve were supposed to be stagnant; and (5) the heating of the cup during the fall was neglected as the fall time was swift.

Solutions were determined using the fully coupled approach, which means that dependent variables were solved simultaneously. Parallel Direct Solver (PARDISO) was used with the automatic Newton's method. Simulations were converged with an absolute tolerance of 10^{-4}. In addition, a sensitivity study of mesh was carried out. A triangular mesh with a maximum element size of 8 mm and a minimum element size of 0.02 mm was firstly used, and the solution was stored. Then the mesh was gradually refined as the new solution still differs from the previous one. Finally, results were not changed when the maximum element size was further reduced to 0.05 mm. Therefore, this element size was retained.

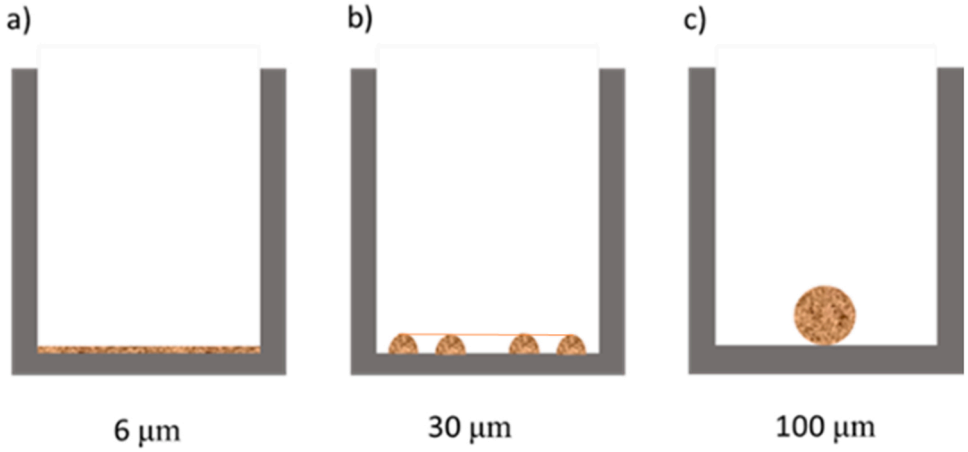

Fig. 4. Different powder arrangements: a) Thin-film with the same diameter as the standard cup, b) torus, and c) sphere.

2.3.1. Geometry

All the components of the pyrolysis system were considered in the model, including the air layers between the heating sleeve and the reactor and between the heating sleeve and the insulator, as it is shown in Fig. 3. All dimensions can be found in Appendix A.

In the model implementation, the cup was slightly raised to allow the passage of helium. A flat bottom also replaced the curved bottom part of the cup. As the actual arrangement of powdered biomass samples at the bottom of the cup is rather difficult to describe, the actual arrangement was bounded between extreme configurations, as it is shown in Fig. 4. The thin-film biomass corresponds to the best configuration for heat transfer as it has a larger surface area in contact with the cup. The sphere refers to the most pessimistic case, and between the two configurations, a more realistic shape can be found, for example, the toroidal one. The indicated characteristic length for each arrangement is the volume of the biomass sample, V_b, divided by its surface, S_b:

$$L_c = \frac{V_b}{S_b} \tag{1}$$

A sample mass of 50 µg was considered in this study as it is often used to prepare biomass thin-film. V_b is therefore calculated for this amount of *Zea mays* powder with a measured bulk density of 409 kg.m^{-3}.

2.3.2. Heat transfer and fluid flow

The model involves conjugate heat transfer coupled with fluid dynamics. The pressure and the velocity field of helium were obtained by resolving mass and momentum equations for a compressible fluid:

$$\frac{\partial \rho}{\partial t} + \nabla.(\rho \boldsymbol{u}) = 0 \tag{2}$$

$$\rho \frac{\partial \mathbf{u}}{\partial t} + \rho \boldsymbol{u} \cdot \nabla \boldsymbol{u} = -\nabla p + \nabla.\left[\mu \left(\nabla \boldsymbol{u} + (\nabla \boldsymbol{u})^T\right) - \frac{2}{3}\mu (\nabla \cdot \boldsymbol{u}) \boldsymbol{I}\right] \tag{3}$$

Where ρ is the density, u is the velocity vector, p is the pressure, μ is the viscosity, the superscript T denotes the transpose operator, and I is the identity matrix.

The flow was assumed to be laminar. This assumption is borne out in the calculations since the average Reynolds number (Re) inside the Quartz tube is always < 20. Temperature fields and heat flux in all parts of the simulation geometry were obtained from the heat equation:

$$\rho C_p \frac{\partial T}{\partial t} + \rho C_p \boldsymbol{u} \cdot \nabla T + \nabla.\boldsymbol{q} = Q + Q_p + Q_{vd} \tag{4}$$

Where C_p and ρ are the heat capacity and the mass density, respectively, T is the temperature, and Q is the heat source term. q, Q_p, and Q_{vd} are respectively the energy source due to conductive (Eq. 5), the pressure (Eq. 6) and viscous dissipation (Eq. 7), and are defined as follows:

$$\boldsymbol{q} = -\lambda \nabla T \tag{5}$$

$$Q_p = \alpha_p T\left(\frac{\partial p}{\partial t} + \boldsymbol{u}.\nabla p\right) \tag{6}$$

$$\mathbf{Q_{vd}} = \boldsymbol{\tau} : \nabla \mathbf{u} \tag{7}$$

Where τ is the viscous stress tensor, and α_p is the coefficient of thermal expansion.

This model also considered radiation heat transfer which was represented as surface-to-surface radiation. Stefan-Boltzman's law was used to model radiative heat flux emitted by diffuse gray surfaces. The considered surfaces were: (1) the outer surfaces of the heating sleeve (emissivity, ε = 0.32); (2) the outer surfaces of the support (ε = 0.8); (3) the outer and inner surfaces of the cup (ε = 0.32); the inner and outer surfaces of the Quartz tube (ε = 0.93); and (4) the outer surface of the biomass sample (ε = 0.9).

The thermophysical proprieties of reactor materials were temperature-dependent as defined in the Comsol databases, except the heating sleeve and the cup, which were considered to have properties of stainless steel with a density of 7960 kg.m^{-3}, heat capacity of 502 J.kg^{-1}. K^{-1}, and thermal conductivity of 16.3 W.m^{-1}. K^{-1}. The thermophysical properties of the biomass used in this work were temperature-dependent, as described by Siddiqi et al. [58].

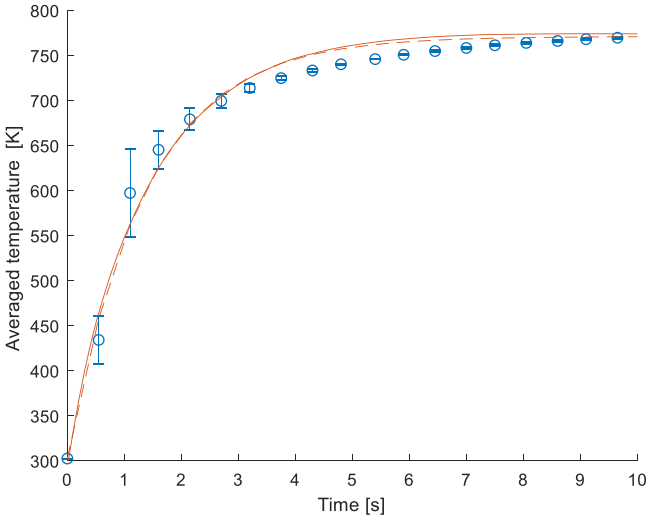

Fig. 5. Time evolution of simulated (Comsol: continuous line, lumped system analysis: dashed line) and measured (circles) cup temperature in the micro-pyrolyzer held at 773 K. Here the standard cup (I.D = 3.6 mm, O.D = 4 mm, and length = 5 mm) was used.

Simulations were carried out in two steps. First, it consisted of determining the temperature fields in the empty micro-reactor at the steady-state before introducing the cup and biomass (see Appendix B). The obtained temperature fields were then used as an initial condition for the transient study when both the cup and biomass sample were added to the problem.

2.3.3. Boundary and initial conditions (transient study)

The continuity of temperature and energy flux at the internal surfaces was ensured by including heat transfer in all simulated geometries, while external surfaces of the reactor were supposed to be thermally insulated. For the transient study, the initial temperatures of cup, biomass, and helium were set to ambient temperature (293 K), while for the rest of the geometries, the temperature fields obtained from the steady-state study were used.

The Helium flow was considered to be laminar. The position of the inlet and outlet to the system are presented in Fig. 3a. The helium inlet velocity was 0.12 m/s at 293 K calculated at the top section of the Quartz tube (I.D = 4.8 mm) for a 125 mL/min fluid flow rate. The outlet pressure was 2.9 bar.

2.3.4. Lumped system analysis

The experimental temperature history of the cup was also fitted to the simple model (lumped system analysis, Eq. 8) based on the approximation of the spatial uniformity of the object temperature during its heating and described by the following equations [59]:

$$\frac{T_{Cup}(t) - T_{Furnace}}{T_0 - T_{Furnace}} = e^{-\frac{t}{\tau}} \tag{8}$$

Where τ is the time constant:

$$\tau = \frac{\rho V C_p}{U A_S} \tag{9}$$

Where $T_{furnace}$ is the temperature of the furnace, T_0 is the initial temperature of the cup, U is the overall heat transfer coefficient at its

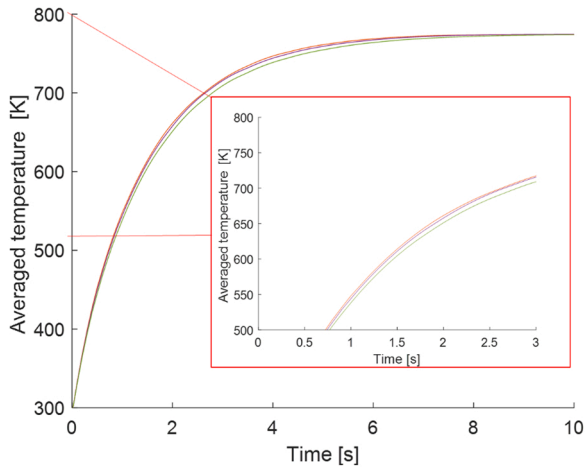

Fig. 6. Simulated temperature vs. time of the cup during heating, taking into account different heat transfer mechanisms and different helium velocities: only conduction in green, conduction + convection (0.12 m/s) in purple, conduction + convection (0.12 m/s) + radiation in orange. Here 0.12 refers to the helium velocity at the top section of the Quartz tube.

surface, A_s is the surface area of the cup, V is the volume of the cup, ρ is its density, and Cp is its specific heat.

3. Results and discussion

3.1. Heating of the cup

The time-temperature history of the cup determined by the finite element method is compared to the experimental one, as it is shown in Fig. 5. A good agreement was observed between the measured and simulated results, then validating the numerical simulation of the micropyrolyzer.

Other simulations were carried out with different cups (see Appendix C) and confirmed that the type of cup did not significantly impact the heat transfer within the reactor.

The time-temperature history of the cup can be described accurately using the simple model (Fig. 5); this indicates that the furnace has a sufficient mass and is not affected by the falling of the cup. The cup is heated as in a fined temperature environment. The heat transfer coefficient at the surfaces of the cup is identified from the simple model and was equal to 335 $W.m^{-2}.K^{-1}$.

The contribution of the different heat transfer mechanisms in the micropyrolyzer was also investigated. Three simulations were therefore carried out: in the first one, only the conduction mechanism was considered (helium was immobile), in the second one, helium flow was added to the problem, and finally, all the mechanisms were considered, including the radiation phenomenon. The time-temperature history of the cup was derived at each simulation, as it is presented in Fig. 6. Adding the helium flow and radiation to the problem does not significantly impact the time evolution of the cup temperature, indicating that conduction is the predominant heat transfer mechanism in the micropyrolyzer.

In the study carried out by Proano et al. [35] using the same micro-reactor and under conditions close to ours (furnace temperature of 773 K and helium velocity at the top section of the Quartz tube of 0.1 m/s), the relative contribution of convection was about 35 %, which differs from our results where convection contribution was negligeable. The difference may be related to the setting of the boundary conditions. In the study of Proano et al. [35], the authors used empirical correlations to determine the boundary conditions at the surface of the cup and imposed temperatures at the outer surface of the Quartz tube, while, in this work, computational fluid dynamics were coupled to heat transfers to avoid these assumptions.

If diffusion in the helium layer between the Quartz tube and the cup is the limiting heat transfer mechanism, at the surface of the cup, we have:

$$\boldsymbol{Q = U * A_s * \left(T_{Furnace} - T_{Cup}(t)\right) = \frac{\left(T_{Furnace} - T_{Cup}(t)\right)}{R}} \tag{10}$$

Where $T_{furnace}$ is the temperature of the furnace, T_{cup} is the temperature of the cup, A_s is the surface area of the cup, U is the overall heat transfer coefficient at its surface, and R is the thermal resistance of the helium layer:

$$\boldsymbol{R = \frac{ln\frac{r_2}{r_1}}{2 * \pi * \lambda * l}} \tag{11}$$

Where r_2 is the internal radius of the Quartz tube, l is the length of the cup and r_1 is the external radius of the cup, and λ is the thermal conductivity of the helium. Then, the overall heat transfer coefficient, U, can be determined without any measurement of cup temperature using the following equation:

$$\boldsymbol{U = \frac{1}{S_{tot}\ R}} \tag{12}$$

The transfer coefficient value of 375 $W.m^{-2}.K^{-1}$ determined using Eq. 12 is comparable to that found using the lumped system analysis.

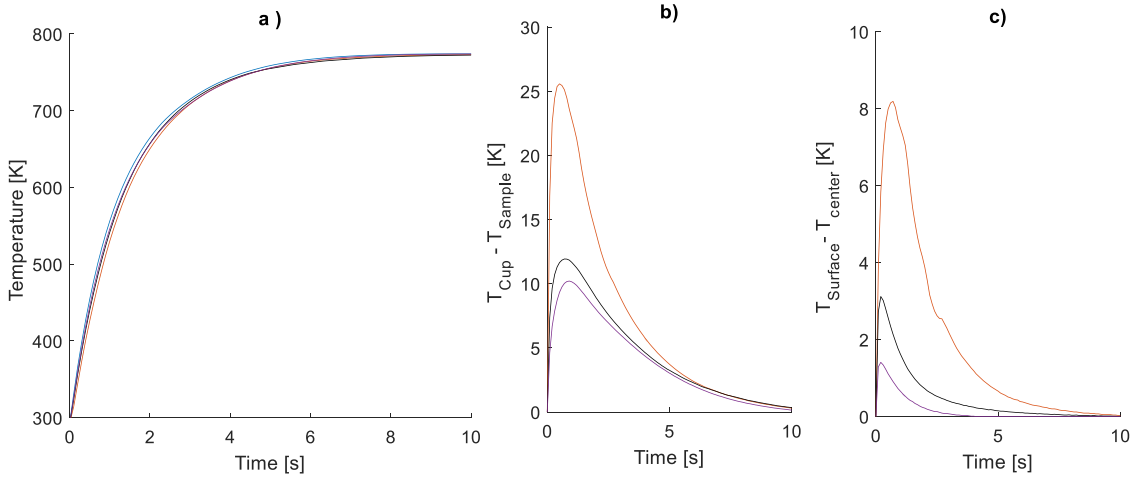

Fig. 7. Heating of the biomass samples in the micropyrolyzer to 773 K. (a) Time-temperature histories of the cup (blue) and biomass samples (sphere: orange, torus: black, and thin-film: purple. (b) Comparison between the cup and samples averaged temperatures and between (c) surface and center temperatures of samples.

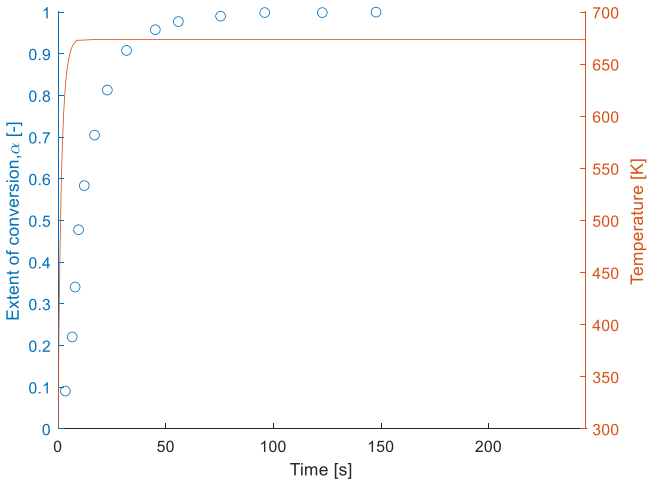

Fig. 8. Conversion curve for cellulose thermal decomposition (on the left) obtained using the Frontier lab micropyrolyzer at 673 K coupled to a mass spectrometer (data were taken from [63]). Simulated temperature history of biomass sample arranged in the form of torus (on the right) obtained at the same conditions of the experiment (of 200 μg of cellulose and helium flow rate of 20 mL/min).

Therefore, the heat transfer is dominated by the heat conduction in the helium layer located between the cup and the Quartz tube; this result reveals that the layer thickness of the helium between the cup and the Quartz tube is so small (0.375 mm) that the cup is heated principally by its side surfaces, absorbing the heat that diffuses through the helium layer.

3.2. Heating of the biomass sample

With the micro-pyrolyzer, it is currently not possible to directly measure the temperature of the biomass sample. However, it can be simulated. Fig. 7 shows the heating of biomass samples with different arrangements. The first observation is that biomass samples approached the reactor temperature within 4–5 s (Fig. 7a). At this high reactor temperature (773 K), the heating time of biomass sample exceeds the time scale of glucose-based carbohydrates fast pyrolysis reaction of 2.5–3 s predicted by the mechanistic model developed by Vinu and Broadbelt [60]. This means that significant biomass conversion took place before the isothermal regime was reached. Thus, an isothermal experiment cannot be claimed; it is essential to consider the sample time-temperature history when studying fast pyrolysis kinetics using the micropyrolyzer. The linearization of the temperature curve cannot be considered as it would introduce unacceptable temperature differences with the actual profile. This is one of the main results of this work. Second, the temperature histories of samples being close to that of the cup (Fig. 5), the temperature differences between samples and the cup (Fig. 7b) was analyzed more carefully. It reveals that the temperatures histories of samples arranged in thin-film and torus were very close to that of the cup with a maximum temperature difference of about 10 and 12 K for thin-film and torus, respectively. However, the maximum temperature difference between the cup and the spherical sample was more than 25 K. Those reported values point out that temperature histories of samples with the suitable arrangement (in the form of thin-film or torus) can be estimated experimentally by measuring the temperature of the cup without going through powerful simulations. However, CFD simulations remain: (1) the best solution in the absence of a precise means of measuring the temperature of the sample to characterize its thermal history and (2) a precise way to deal with more realistic sample arrangements and particles shapes. The heat of the chemical reaction taken into account as a source term in the simulation (see Appendix D) did not affect the heating of a small amount of sample. However, the heat of the reaction needs to be taken into account for larger amounts of sample [61].

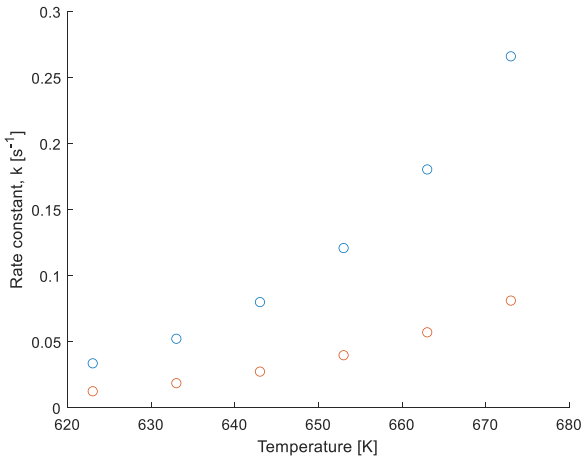

Fig. 9. Direct plots of the thermal decomposition of cellulose at isothermal (blue) and non-isothermal (orange) conditions.

Table 2
Averaged heat transfer coefficients over the surface of samples with different arrangements.

	At $T_{furnace}$ = 623 K	At $T_{furnace}$ = 673 K	At $T_{furnace}$ = 723 K	At $T_{furnace}$ = 773 K
Thin film	205	217	225	244
Torus	197	203	214	235
Sphere	165	183	199	208

If internal heat transfer existed, the sample center temperature would be significantly lower than the surface temperature. As it is shown in Fig. 7c, a minor temperature inhomogeneity within samples with different arrangements ($T_{surface} - T_{center} < 8$ K) indicates a negligible effect of the internal heat transfer in the micropyrolyzer.

3.3. Influence of the temperature profile on reaction rate

In recent years, few studies have started to publish fast pyrolysis kinetics datasets using analytical pyrolysis instruments under isothermal conditions without verifying the isothermal nature of the experiment [29,62–64]. In this paper, the non-isothermal character of biomass fast pyrolysis using the micropyrolyzer is confirmed, and a non-isothermal kinetic approach is required. This verification work is essential to avoid the use of incorrect kinetics datasets. As shown in Fig. 8, more than 20% of biomass conversion was attaint before reaching the set temperature of 673 K.

The reaction rate of cellulose pyrolysis (Fig. 9) determined according a first-order model and the temperature history of the biomass sample (see calculation details in Appendix E) confirms that the constant rate at 673 K is increased 3.3 times when considering the non-isothermal character of the reaction; a factor that is equal to 4.7 when the constant rate is 3 times faster.

3.4. Rate regime determination

Now that the thermal history of the particle is known, the effect of external heat transfers are about to be examined through a dimensional analysis. Both heat transfer coefficients at the surface of different sample arrangements (Table 2) were determined using numerical simulations, as it is described in Appendix F. The obtained values were between 165 and 244 W.m^{-2}. K^{-1} for different sample arrangements and temperatures (623–773 K) and were smaller than those usually used to calculate

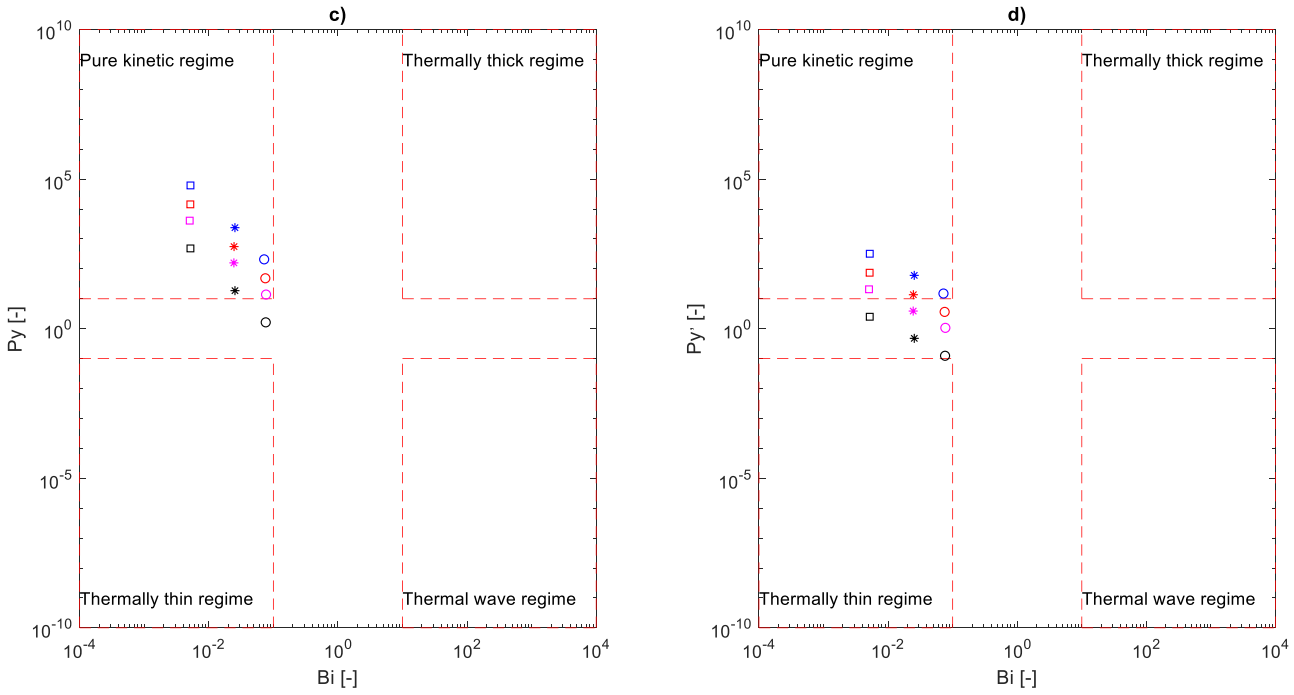

Fig. 10. Reaction-transport map for biomass fast pyrolysis of 50 µg of biomass sample with different arrangements (thin- film: rectangles, torus: stars, and sphere: circles) at different temperatures (623 K: blue, 673 K: red, 723 K: magenta, and 773 K: black). a) Py vs. Bi and b) Py' vs. Bi. Here biomass thermophysical properties were used[58].

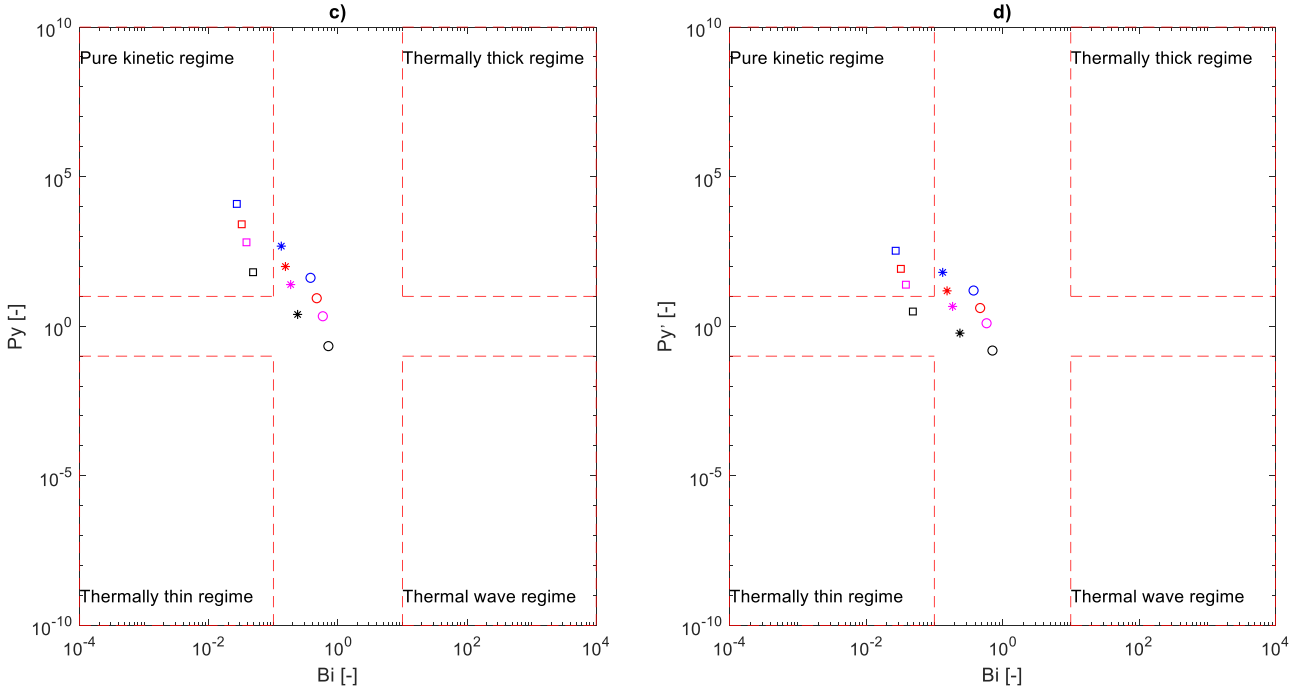

Fig. 11. Reaction-transport map for biomass fast pyrolysis of 50 µg of biomass sample with different arrangements (thin- film: rectangles, torus: stars, and sphere: circles) at different temperatures (623 K: blue, 673 K: red, 723 K: magenta, and 773 K: black). a) Py vs. Bi and b) Py' vs. Bi. Here char thermophysical properties were used [65].

the dimensionless number. Biot and pyrolysis numbers were calculated using the obtained heat transfer coefficients, the rate constants of reaction taken from experiments using the PHASR reactor [41], and biomass thermophysical properties obtained from Siddiqi et al. [58].

Pyrolysis transport maps (Fig. 10) display both pyrolysis numbers, Py (the ration between reaction and conduction time scales) and Py'(the ration between reaction and convection time scales), versus the Biot number (the ration between conduction and external heat time scales) for the three 50 µg biomass sample arrangements and at different micro-reactor temperatures (623–773 K).

It shows that for all the sample arrangements, the points were in an intrinsic kinetic zone except for the sphere at a temperature of 773 K.

Thus, the internal transfers are faster than the reaction. Their effect is negligible for this experimental device, especially for arrangement in the form of the thin-film or torus.

On the other hand, the examination of Py' as a function of Biot (Fig. 10 b) indicates that both the arrangement of the sample and the temperature play a critical role in external heat transfer limitations. The sample at the bottom of the cup must be carefully arranged to approximate the thin-film configuration, or ideally, one can use the thin-film technique discussed in the introduction to ensure an intrinsic kinetic regime. It is also important to note that the temperature needs to be smaller than 723 K as all the points are outside the pure kinetics zone at 773 K.

During pyrolysis, biomass is converted into volatile products and biochar. Therefore, the thermophysical properties of the reactive solid material change with time. For the most pessimistic case investigation, dimensionless numbers were calculated with the biochar thermophysical properties, as it is a poor conductor of heat. Thermophysical properties of biochar were taken from Babu et al.[65]. As expected, the low thermal conductivity of biochar leads to low biot numbers and shifts the points to the right zone (Fig. 11) where the internal heat transfer within the particle start to control the process.

It is shown that only points for thin-film biomass remained in the intrinsic kinetic zone. Thus, thin-film biomass was the most favorable arrangement to establish a kinetic regime. Heat transfer limitations logically become more noticeable for larger masses. An amount of 50 µg appears as the maximum sample mass to be used to study the intrinsic kinetics of biomass fast pyrolysis.

4. Conclusions

Numerical simulations were carried out to provide insights into heat transfers to and within the biomass samples in the micropyrolyzer. These simulations indicated that conductive heat dominates heat transfer to the cup and the biomass samples. They provided information that is non-accessible experimentally, such as the temperature history of the biomass sample and the heat transfer coefficients at its surface (165–244 $W.m^{-2}.K^{-1}$). This work demonstrates that micropyrolyzer kinetics of biomass fast pyrolysis can be carried out without heat transfers limitations by using small masses of biomass samples ($\leq$ 50 µg), carefully arranged on the bottom of the cup. The heating time of biomass was significant, indicating a non-isothermal nature of the experiment. Therefore, kinetics analysis requires establishing the biomass sample temperature history, which can be determined by measuring the cup temperature. At temperatures above 723 K, the reaction is so fast that the pure kinetic regime cannot be maintained.

Declaration of Competing Interest

The authors declare that they have no known competing financial interests or personal relationships that could have appeared to influence the work reported in this paper.

Acknowledgments

The authors acknowledge the French Scientific Program MOPGA (reference ANR-18-MPGA-0013) managed by the National Research Agency and financially supported by the "Investissements d'Avenir" and Region Occitanie (18016004). We acknowledge the helpful advices of Dr. Olivier Louisnard.

Appendix A. Supporting information

Supplementary data associated with this article can be found in the online version at doi:10.1016/j.jaap.2022.105582.

References

[1] B.V. Babu, Biomass pyrolysis: a state-of-the-art review, Biofuels Bioprod. Bioref. 2 (2008) 393–414, https://doi.org/10.1002/bbb.92.
[2] A.V. Bridgwater, Review of fast pyrolysis of biomass and product upgrading, Biomass Bioenergy 38 (2012) 68–94, https://doi.org/10.1016/j.biombioe.2011.01.048.
[3] Y.H. Chan, S.K. Loh, B.L.F. Chin, C.L. Yiin, B.S. How, K.W. Cheah, M.K. Wong, A.C. M. Loy, Y.L. Gwee, S.L.Y. Lo, S. Yusup, S.S. Lam, Fractionation and extraction of bio-oil for production of greener fuel and value-added chemicals: recent advances and future prospects, Chem. Eng. J. 397 (2020), 125406, https://doi.org/10.1016/j.cej.2020.125406.
[4] S.S. Chen, T. Maneerung, D.C.W. Tsang, Y.S. Ok, C.-H. Wang, Valorization of biomass to hydroxymethylfurfural, levulinic acid, and fatty acid methyl ester by heterogeneous catalysts, Chem. Eng. J. 328 (2017) 246–273, https://doi.org/10.1016/j.cej.2017.07.020.
[5] T. Bridgwater, Challenges and opportunities in fast pyrolysis of biomass: Part I, Johns. Matthey Technol. Rev. 62 (2018) 118–130, https://doi.org/10.1595/205651318×696693.
[6] D. Beneroso, T. Monti, E.T. Kostas, J. Robinson, Microwave pyrolysis of biomass for bio-oil production: scalable processing concepts, Chem. Eng. J. 316 (2017) 481–498, https://doi.org/10.1016/j.cej.2017.01.130.
[7] T.M.H. Dabros, M.Z. Stummann, M. Høj, P.A. Jensen, J.-D. Grunwaldt, J. Gabrielsen, P.M. Mortensen, A.D. Jensen, Transportation fuels from biomass fast pyrolysis, catalytic hydrodeoxygenation, and catalytic fast hydropyrolysis, Prog. Energy Combust. Sci. 68 (2018) 268–309, https://doi.org/10.1016/j.pecs.2018.05.002.
[8] G. Perkins, T. Bhaskar, M. Konarova, Process development status of fast pyrolysis technologies for the manufacture of renewable transport fuels from biomass, Renew. Sustain. Energy Rev. 90 (2018) 292–315, https://doi.org/10.1016/j.rser.2018.03.048.
[9] J. Lédé, Cellulose pyrolysis kinetics: an historical review on the existence and role of intermediate active cellulose, J. Anal. Appl. Pyrolysis 94 (2012) 17–32, https://doi.org/10.1016/j.jaap.2011.12.019.
[10] M.S. Mettler, D.G. Vlachos, P.J. Dauenhauer, Top ten fundamental challenges of biomass pyrolysis for biofuels, Energy Environ. Sci. 5 (2012) 7797, https://doi.org/10.1039/c2ee21679e.
[11] M.S. Mettler, S.H. Mushrif, A.D. Paulsen, A.D. Javadekar, D.G. Vlachos, P. J. Dauenhauer, Revealing pyrolysis chemistry for biofuels production: conversion of cellulose to furans and small oxygenates, Energy Environ. Sci. 5 (2012) 5414–5424, https://doi.org/10.1039/c1ee02743c.
[12] M.B. Pecha, J.I.M. Arbelaez, M. Garcia-Perez, F. Chejne, P.N. Ciesielski, Progress in understanding the four dominant intra-particle phenomena of lignocellulose pyrolysis: chemical reactions, heat transfer, mass transfer, and phase change, Green. Chem. 21 (2019) 2868–2898, https://doi.org/10.1039/C9GC00585D.
[13] P.J. Dauenhauer, J.L. Colby, C.M. Balonek, W.J. Suszynski, L.D. Schmidt, Reactive boiling of cellulose for integrated catalysis through an intermediate liquid, Green Chem. 11 (2009) 1555, https://doi.org/10.1039/b915068b.
[14] Z. Ma, D. Chen, J. Gu, B. Bao, Q. Zhang, Determination of pyrolysis characteristics and kinetics of palm kernel shell using TGA-FTIR and model-free integral methods, Energy Convers. Manag. 89 (2015) 251–259, https://doi.org/10.1016/j.enconman.2014.09.074.
[15] A.A. Jain, A. Mehra, V.V. Ranade, Processing of TGA data: analysis of isoconversional and model fitting methods, Fuel 165 (2016) 490–498, https://doi.org/10.1016/j.fuel.2015.10.042.
[16] S. Maduskar, G.G. Facas, C. Papageorgiou, C.L. Williams, P.J. Dauenhauer, Five rules for measuring biomass pyrolysis rates: pulse-heated analysis of solid reaction kinetics of lignocellulosic biomass, ACS Sustain. Chem. Eng. 6 (2018) 1387–1399, https://doi.org/10.1021/acssuschemeng.7b03785.
[17] E. Hoekstra, W.P.M. Van Swaaij, S.R.A. Kersten, K.J.A. Hogendoorn, Fast pyrolysis in a novel wire-mesh reactor: decomposition of pine wood and model compounds, Chem. Eng. J. 187 (2012) 172–184, https://doi.org/10.1016/j.cej.2012.01.118.
[18] E. Hoekstra, W.P.M. van Swaaij, S.R.A. Kersten, K.J.A. Hogendoorn, Fast pyrolysis in a novel wire-mesh reactor: design and initial results, Chem. Eng. J. 191 (2012) 45–58, https://doi.org/10.1016/j.cej.2012.01.117.
[19] C. Krumm, J. Pfaendtner, P.J. Dauenhauer, Millisecond Pulsed Films Unify the Mechanisms of Cellulose Fragmentation, (n.d.) 39.
[20] P.R. Patwardhan, J.A. Satrio, R.C. Brown, B.H. Shanks, Product distribution from fast pyrolysis of glucose-based carbohydrates, J. Anal. Appl. Pyrolysis 86 (2009) 323–330, https://doi.org/10.1016/j.jaap.2009.08.007.
[21] P.R. Patwardhan, R.C. Brown, B.H. Shanks, Product distribution from the fast pyrolysis of hemicellulose, ChemSusChem 4 (2011) 636–643, https://doi.org/10.1002/cssc.201000425.
[22] G. Liu, M.M. Wright, Q. Zhao, R.C. Brown, Catalytic fast pyrolysis of duckweed: Effects of pyrolysis parameters and optimization of aromatic production, J. Anal. Appl. Pyrolysis 112 (2015) 29–36, https://doi.org/10.1016/j.jaap.2015.02.026.
[23] M.K. Akalın, S. Karagöz, Analytical pyrolysis of biomass using gas chromatography coupled to mass spectrometry, TrAC Trends Anal. Chem. 61 (2014) 11–16, https://doi.org/10.1016/j.trac.2014.06.006.
[24] T.U. Han, Y.-M. Kim, M.Z. Siddiqui, T. Lee, A. Watanabe, N. Teramae, S. Kim, Y.-K. Park, Non-isothermal pyrolysis properties of Laminaria japonica, J. Anal. Appl. Pyrolysis 130 (2018) 277–284, https://doi.org/10.1016/j.jaap.2017.12.021.
[25] F. Nardella, M. Mattonai, E. Ribechini, Evolved gas analysis-mass spectrometry and isoconversional methods for the estimation of component-specific kinetic data in wood pyrolysis, J. Anal. Appl. Pyrolysis 145 (2020), 104725, https://doi.org/10.1016/j.jaap.2019.104725.

[26] F.-S. Lin, T.-S. Chang, M.-H. Rei, Rapid pyrolysis of rice hull in a curie-point pyrolyzer, Agric. Wastes 18 (1986) 103–121, https://doi.org/10.1016/0141-4607(86)90003-X.

[27] S. Lee, Y.-M. Kim, M.Z. Siddiqui, Y.-K. Park, Different pyrolysis kinetics and product distribution of municipal and livestock manure sewage sludge, Environ. Pollut. 285 (2021), 117197, https://doi.org/10.1016/j.envpol.2021.117197.

[28] L. Hu, X.-Y. Wei, X.-H. Guo, H.-P. Lv, G.-H. Wang, Investigation on the kinetic behavior, thermodynamic and volatile products analysis of chili straw waste pyrolysis, J. Environ. Chem. Eng. 9 (2021), 105859, https://doi.org/10.1016/j.jece.2021.105859.

[29] D.K. Ojha, D. Viju, R. Vinu, Fast pyrolysis kinetics of lignocellulosic biomass of varying compositions, Energy Convers. Manag. X 10 (2021), 100071, https://doi.org/10.1016/j.ecmx.2020.100071.

[30] E. Biagini, F. Lippi, L. Tognotti, Characterization of a lab-scale platinum filament pyrolyzer for studying the fast devolatilization of solid fuels, Fuel 85 (2006) 2408–2418, https://doi.org/10.1016/j.fuel.2006.06.002.

[31] A. Rastogi, W.Y. Svrcek, L.A. Behie, The importance of temperature rise time in pyrolysis kinetic studies, Can. J. Chem. Eng. 66 (1988) 303–306, https://doi.org/10.1002/cjce.5450660218.

[32] A. Alves, M. Schwanninger, H. Pereira, J. Rodrigues, Analytical pyrolysis as a direct method to determine the lignin content in wood, J. Anal. Appl. Pyrolysis 76 (2006) 209–213, https://doi.org/10.1016/j.jaap.2005.11.004.

[33] B. Scholze, D. Meier, Characterization of the water-insoluble fraction from pyrolysis oil (pyrolytic lignin). Part I. PY–GC/MS, FTIR, and functional groups, J. Anal. Appl. Pyrolysis 60 (2001) 41–54, https://doi.org/10.1016/S0165-2370(00)00110-8.

[34] Q. Lu, Z.-F. Zhang, C.-Q. Dong, X.-F. Zhu, Catalytic upgrading of biomass fast pyrolysis vapors with nano metal oxides: an analytical Py-GC/MS study, Energies 3 (2010) 1805–1820, https://doi.org/10.3390/en3111805.

[35] J. Proano-Aviles, J.K. Lindstrom, P.A. Johnston, R.C. Brown, Heat and mass transfer effects in a furnace-based micropyrolyzer, Energy Technol. 5 (2017) 189–195, https://doi.org/10.1002/ente.201600279.

[36] S. Vyazovkin, A.K. Burnham, J.M. Criado, L.A. Pérez-Maqueda, C. Popescu, N. Sbirrazzuoli, ICTAC kinetics committee recommendations for performing kinetic computations on thermal analysis data, Thermochim. Acta 520 (2011) 1–19, https://doi.org/10.1016/j.tca.2011.03.034.

[37] M.B. Pecha, J.I.M. Arbelaez, M. Garcia-Perez, F. Chejne, P.N. Ciesielski, Progress in understanding the four dominant intra-particle phenomena of lignocellulose pyrolysis: chemical reactions, heat transfer, mass transfer, and phase change, Green Chem. 21 (2019) 2868–2898, https://doi.org/10.1039/C9GC00585D.

[38] J. Zhang, M.W. Nolte, B.H. Shanks, Investigation of primary reactions and secondary effects from the pyrolysis of different celluloses, ACS Sustain. Chem. Eng. 2 (2014) 2820–2830, https://doi.org/10.1021/sc500592v.

[39] M.S. Mettler, D.G. Vlachos, P.J. Dauenhauer, Top ten fundamental challenges of biomass pyrolysis for biofuels, Energy Environ. Sci. 5 (2012) 7797, https://doi.org/10.1039/c2ee21679e.

[40] A.D. Paulsen, M.S. Mettler, P.J. Dauenhauer, The role of sample dimension and temperature in cellulose pyrolysis, Energy Fuels 27 (2013) 2126–2134, https://doi.org/10.1021/ef302117j.

[41] C. Zhu, C. Krumm, G.G. Facas, M. Neurock, P.J. Dauenhauer, Energetics of cellulose and cyclodextrin glycosidic bond cleavage, React. Chem. Eng. 2 (2017) 201–214, https://doi.org/10.1039/C6RE00176A.

[42] G. SriBala, H.-H. Carstensen, K.M. Van Geem, G.B. Marin, Measuring biomass fast pyrolysis kinetics: state of the art, WIREs Energy Environ. 8 (2019), e326, https://doi.org/10.1002/wene.326.

[43] D.L. Brink, M.S. Massoudi, Flow reactor technique for the study of wood pyrolysis. I. experimental, J. Fire Flammabl. 9 (1978). ⟨https://www.osti.gov/etdeweb/biblio/5038259⟩. accessed August 9, 2021.

[44] F. Thurner, U. Mann, Kinetic investigation of wood pyrolysis, (n.d.) 7.

[45] D.L. Pyle, C.A. Zaror, Heat transfer and kinetics in the low temperature pyrolysis of solids, Chem. Eng. Sci. 39 (1984) 147–158, https://doi.org/10.1016/0009-2509(84)80140-2.

[46] R. Font, A. Marcilla, E. Verdú, J. Devesa, Thermogravimetric kinetic study of the pyrolysis of almond shells and almond shells impregnated with CoCl2, J. Anal. Appl. Pyrolysis 21 (1991) 249–264, https://doi.org/10.1016/0165-2370(91)80001-O.

[47] B.M. Wagenaar, W. Prins, W.P.M. van Swaaij, Flash pyrolysis kinetics of pine wood, Fuel Process. Technol. 36 (1993) 291–298, https://doi.org/10.1016/0378-3820(93)90039-7.

[48] C. Di Blasi, C. Branca, Kinetics of Primary Product Formation from Wood Pyrolysis, Ind. Eng. Chem. Res. 40 (2001) 5547–5556, https://doi.org/10.1021/ie000997e.

[49] A. Anca-Couce, Reaction mechanisms and multi-scale modelling of lignocellulosic biomass pyrolysis, Prog. Energy Combust. Sci. 53 (2016) 41–79, https://doi.org/10.1016/j.pecs.2015.10.002.

[50] D.L. Pyle, C.A. Zaror, Heat transfer and kinetics in the low temperature pyrolysis of solids, Chem. Eng. Sci. 39 (1984) 147–158, https://doi.org/10.1016/0009-2509(84)80140-2.

[51] M. Carrier, M. Windt, B. Ziegler, J. Appelt, B. Saake, D. Meier, A. Bridgwater, Quantitative insights into the fast pyrolysis of extracted cellulose, hemicelluloses, and lignin, ChemSusChem 10 (2017) 3212–3224, https://doi.org/10.1002/cssc.201700984.

[52] K. Papadikis, S. Gu, A.V. Bridgwater, CFD modelling of the fast pyrolysis of biomass in fluidised bed reactors: modelling the impact of biomass shrinkage, Chem. Eng. J. 149 (2009) 417–427, https://doi.org/10.1016/j.cej.2009.01.036.

[53] E. Mielke, P. Plouffe, N. Koushik, M. Eyholzer, M. Gottsponer, N. Kockmann, A. Macchi, D.M. Roberge, Local and overall heat transfer of exothermic reactions in microreactor systems, React. Chem. Eng. 2 (2017) 763–775, https://doi.org/10.1039/C7RE00085E.

[54] J. Wang, M. Wang, Z. Li, A lattice Boltzmann algorithm for fluid–solid conjugate heat transfer, Int. J. Therm. Sci. 46 (2007) 228–234, https://doi.org/10.1016/j.ijthermalsci.2006.04.012.

[55] A. Dorfman, Z. Renner, Conjugate problems in convective heat transfer: review, Math. Probl. Eng. 2009 (2009) 1–27, https://doi.org/10.1155/2009/927350.

[56] Q. Xiong, S.-C. Kong, High-resolution particle-scale simulation of biomass pyrolysis, ACS Sustain. Chem. Eng. 4 (2016) 5456–5461, https://doi.org/10.1021/acssuschemeng.6b01020.

[57] Q. Xiong, F. Xu, Y. Pan, Y. Yang, Z. Gao, S. Shu, K. Hong, F. Bertrand, J. Chaouki, Major trends and roadblocks in CFD-aided process intensification of biomass pyrolysis, Chem. Eng. Process. - Process. Intensif. 127 (2018) 206–212, https://doi.org/10.1016/j.cep.2018.04.005.

[58] H. Siddiqi, U. Kumari, S. Biswas, A. Mishra, B.C. Meikap, A synergistic study of reaction kinetics and heat transfer with multi-component modelling approach for the pyrolysis of biomass waste, Energy 204 (2020), 117933, https://doi.org/10.1016/j.energy.2020.117933.

[59] F.P. Incropera, F.P. Incropera. Fundamentals of Heat and Mass Transfer, Sixthth ed., John Wiley, Hoboken, NJ, 2007.

[60] R. Vinu, L.J. Broadbelt, A mechanistic model of fast pyrolysis of glucose-based carbohydrates to predict bio-oil composition, Energy Environ. Sci. 5 (2012) 9808–9826, https://doi.org/10.1039/C2EE22784C.

[61] C.Di Blasi, Kinetic and heat transfer control in the slow and flash pyrolysis of solids, Ind. Eng. Chem. Res. 35 (1996) 37–46, https://doi.org/10.1021/ie950243d.

[62] J.V. Jayarama Krishna, O.P. Korobeinichev, R. Vinu, Isothermal fast pyrolysis kinetics of synthetic polymers using analytical Pyroprobe, J. Anal. Appl. Pyrolysis 139 (2019) 48–58, https://doi.org/10.1016/j.jaap.2019.01.008.

[63] N. Phusunti, A. Hornung, 2014. Formal Kinetic Parameters – Problems and Solutions in Deriving Proper Values, (2014) 257–284. ⟨https://doi.org/10.1002/9781118693643.ch14⟩.

[64] D.K. Ojha, D. Viju, R. Vinu, Fast pyrolysis kinetics of alkali lignin: Evaluation of apparent rate parameters and product time evolution, Bioresour. Technol. 241 (2017) 142–151, https://doi.org/10.1016/j.biortech.2017.05.084.

[65] B.V. Babu, A.S. Chaurasia, Parametric study of thermal and thermodynamic properties on pyrolysis of biomass in thermally thick regime, Energy Convers. Manag. 45 (2004) 53–72, https://doi.org/10.1016/S0196-8904(03)00130-4.